Energetics and Geometry of FtsZ Polymers: Nucleated Self-Assembly of Single Protofilaments

Sonia Huecas,* Oscar Llorca,* Jasminka Boskovic,* Jaime Martín-Benito,† José María Valpuesta,† and José Manuel Andreu*

*Centro de Investigaciones Biológicas, Madrid, Spain; and †Centro Nacional de Biotecnología, Madrid, Spain

ABSTRACT Essential cell division protein FtsZ is an assembling GTPase which directs the cytokinetic ring formation in dividing bacterial cells. FtsZ shares the structural fold of eukaryotic tubulin and assembles forming tubulin-like protofilaments, but does not form microtubules. Two puzzling problems in FtsZ assembly are the nature of protofilament association and a possible mechanism for nucleated self-assembly of single-stranded protofilaments above a critical FtsZ concentration. We assembled two-dimensional arrays of FtsZ on carbon supports, studied linear polymers of FtsZ with cryo-electron microscopy of vitrified unsupported solutions, and formulated possible polymerization models. Nucleated self-assembly of FtsZ from *Escherichia coli* with GTP and magnesium produces flexible filaments 4–6 nm-wide, only compatible with a single protofilament. This agrees with previous scanning transmission electron microscopy results and is supported by recent cryo-electron tomography studies of two bacterial cells. Observations of double-stranded FtsZ filaments in negative stain may come from protofilament accretion on the carbon support. Preferential protofilament cyclization does not apply to FtsZ assembly. The apparently cooperative polymerization of a single protofilament with identical intermonomer contacts is explained by the switching of one inactive monomer into the active structure preceding association of the next, creating a dimer nucleus. FtsZ behaves as a cooperative linear assembly machine.

INTRODUCTION

Essential cell division protein FtsZ, a self-assembling GTPase, localizes to the midcell (1) where it recruits the other prokaryotic divisome proteins (2–6). FtsZ and eukaryotic tubulin share the same structural fold and form similar protofilaments (7,8), but the lateral interactions of tubulin that generate microtubules (9) and the capacity to bind to eukaryotic cytosolic chaperonin CCT are absent in the shorter surface loops of FtsZ which, unlike $\alpha\beta$-tubulin, can fold spontaneously (10–12). Both FtsZ polymers and microtubules use GTP hydrolysis to disassemble (13–15), and the former's dynamics is of seconds (16,17). However, if the nucleotide remains exchangeable, FtsZ polymers (8,18,19) may not share the microtubule dynamic instability mechanism (20).

Once the septum between daughter cells has constricted, the FtsZ ring disappears. Fluorescence microscopy images suggest that it may be a compressed helix (21,22), which has not shown up in conventional EM visualization. An important question is how FtsZ protofilaments associate to form physiological FtsZ polymers. FtsZ polymerizes in vitro (23,24), forming contrasting structures in which protofilaments associate in different fashions. Single protofilaments were observed by scanning transmission electron microscopy (STEM), electron microscopy (EM) after negative stain, and atomic force microscopy (AFM) (19,25–28). Double protofilaments, bundles, and ribbons were also observed by EM (29–35).

We characterized an FtsZ double-stranded filament and proposed this as its primary assembly product (33), which would explain FtsZ apparently cooperative polymerization taking place abruptly above a critical protein concentration (36). Erickson and co-workers proposed a single protofilament based on STEM measurements (25) but could not explain their observed cooperative kinetics with a dimer nucleus (26). Gonzalez et al. (27) came up with a proposal of preferential cyclization of single-stranded filaments to explain cooperative behavior, based on sedimentation velocity results. One concern is that sample adsorption from solution on the EM support may have perturbed FtsZ polymer structure in the various studies by modifying the degree of lateral association of protofilaments. Therefore, it becomes necessary to determine the structure of unperturbed FtsZ polymers in vitro and in cells. Recently, two electron tomography studies reported the observation in two unfixed bacterial cells of 5 nm cytoplasmic fibers suggestive of single FtsZ protofilaments (37,38).

The structural principles of protein self-assembly machines were set by Caspar, Klug, and colleagues (39–41), based on Crick and Watson's suggestion that simple virus shells are made up of identical, regularly packed protein subunits (42). The thermodynamics of nucleated condensation protein polymerization, including helical assembly of actin, established by Oosawa and co-workers (43,44), has been extended and applied many times to the assembly of cytoskeletal protein fibers (45–52). The principles of biological self-assembly have also been applied to synthetic systems (53). Linear isodesmic

Submitted June 21, 2007, and accepted for publication October 31, 2007.

Address reprint requests to J. M. Andreu, Tel.: 34-91-837-3112, ext 4381; E-mail: j.m.andreu@cib.csic.es.

J. Boskovic's current address is Centro Nacional de Investigaciones Oncológicas, Melchor Fernandez Almagro, 3, 28029 Madrid, Spain.

Editor: Edward H. Egelman.

0006-3495/08/03/1796/11 $2.00

doi: 10.1529/biophysj.107.115493

protein self-association typically proceeds with practically constant affinity at each association step, since an identical bond is formed. This results in the rapid formation of polymers of various lengths coexisting with monomers; polymers form from low protein concentrations, and their average length and the monomer concentration gradually increase with total protein concentration. In contrast, nucleated polymerization is characterized by a significantly smaller affinity for nucleation than for polymer elongation; additional bonds may be formed but are not necessary, as will be shown below. This results in the formation of long polymers in equilibrium with monomers, and an insignificant concentration of intermediate species. Typical features of nucleated polymerization include polymer formation with a sigmoidal time-course after a nucleation lag time, and that polymers are observed only above a given critical total protein concentration C_r, from which point the monomer concentration remains equal to C_r, and all excess protein goes into polymers. The value of C_r is in good approximation equal to the reciprocal value of the equilibrium elongation constant of the polymer (44). Multistranded protein polymers are usually observed to assemble above a critical concentration apparently following a nucleated condensation mechanism (44), whereas single-stranded indefinite polymerization has been considered necessarily isodesmic (25).

Nucleotide hydrolysis and exchange coupled to polymerization adds dynamics to protein assembly (45). Dynamic nucleated polymerization of cytoskeletal fibers can be employed in a cell to control assembly of complex subcellular machines by providing cues for nucleation, stabilization, or depolymerization at certain positions and times (54,55), which would work less efficiently with isodesmic assembly. Steady-state polymers in nucleotide excess can still be studied with equilibrium methods, or hydrolysis can be inhibited under particular conditions or with nonhydrolyzable nucleotide analogs.

This work aims to better define the structure of polymers formed by purified FtsZ and to reconcile it with assembly energetics. Two-dimensional (2D) crystallization of FtsZ has been investigated. Linear polymers of FtsZ in solution have been studied with cryo-electron microscopy (cryo-EM) for the first time to our knowledge, and a mechanism explaining the observations of nucleated polymerization of single-stranded FtsZ filaments is formulated.

EXPERIMENTAL METHODS

Polymerization of *Methanococcus jannaschii* FtsZ-W319Y-His$_6$ on grids and EM

The histidine-tagged W319Y mutant of FtsZ from the hyperthermophile *M. jannaschii* was expressed in *E. coli*, affinity-purified, and its concentration determined (33). Stock protein (~50 g L^{-1}, containing 0.6 bound guanine nucleotide per FtsZ) was melted and diluted to 0.8–1 g L^{-1} into 50 mM Mes/KOH, 50 mM KCl, 1 mM EDTA, buffer pH 6.5, at 40–45°C (the His-tagged protein has a tendency to precipitate in this buffer at room temperature). The solution was clarified at 50,000 rpm, 10 min, in a TLA120.2 rotor (Beckman, Fullerton, CA) at 40°C. The FtsZ-W319Y concentration in the supernatant (0.6–0.8 g L^{-1}) was measured spectrophotometrically, employing a practical extinction coefficient value of 0.165 g^{-1} L cm^{-1} at 280 nm (0.224 g^{-1} L cm^{-1} at 254 nm; determined by reference to the stock concentration), and the protein was kept warm. Aliquots of the solution (100 μL) with an EM grid as either a carbon holey grid (Quantifoil Micro Tools, Jena, Germany) or a carbon-coated grid (Quantifoil) floating upside down, were dialyzed against the same buffer plus 12 mM $MgCl_2$ and 1 mM GDP (1 mL), at 45°C (measured with a thin thermocouple in a parallel sample), during 3.5 h or overnight, employing capped mini-dialysis units (model No. 69570, 10,000 MW cutoff; Pierce, Rockford, IL) placed in 1.5 ml open tubes in a ThermoStat Plus (set to 49°C, no shaking; Eppendorf, Hamburg, Germany).

Protein samples adsorbed on the grids were negatively stained with 2% uranyl acetate, or immediately processed for cryo-EM. FtsZ sheets were localized at low magnification (~2500×) and photographed at higher magnification, employing a model No. 1230 electron microscope (Jeol, Tokyo, Japan) or a G^2 FEG 200 electron microscope (Tecnai, Hillsboro, OR) equipped with a cold stage (Gatan, Pleasanton, CA) operated at 200 kV. Micrographs for image reconstruction were acquired under low-dose conditions. Cryo-electron micrographs were recorded on SO-163 film (Kodak, Rochester, NY) at 62,000× nominal magnification and between 1.5 and 2.5 μm underfocus. The best images, as judged by optical diffraction, were digitized in a SCAI scanner (Zeiss, Jena, Germany) with a sampling window corresponding to 0.14 nm/pixel. Lattice refinement of the images was carried out using the X-windows-based graphical environment SPECTRA (56) and the subsequent image processing, including lattice unbending, was performed using the MRC image processing suite (57). Transfer function correction was carried out using the Integrated Crystallographic Environment (58). Images were merged with the program ORIGTILT (57), with the use of the crystallographic group $p222_1$, as suggested by the program ALLSPACE (59).

Cryo-EM of *Escherichia coli* FtsZ polymers on holey films

FtsZ was overproduced and purified with two cycles of calcium precipitation followed by ion exchange (32). FtsZ polymers were assembled in buffers specified at 30°C and quantified by isothermal pelleting 15 min at 80,000 rpm in a prewarmed model No. TLA100 rotor (Beckman) with 7 × 20 mm tubes (36). Circular dichroism spectra were collected as described (36) employing a 0.2 mm cell at 30°C.

A few microliters of *E. coli* FtsZ polymer solution were applied to holey-film grids (Quantifoil) after glow-discharge and immediately blotted and vitrified by plunging into liquid ethane. Two types of samples were vitrified. Sample 1: FtsZ (12 μM) in 50 mM Mes-KOH, 50 mM KCl, 1 mM EDTA, 6 mM magnesium acetate, and 1 mM GTP, pH 6.5 (Mes buffer). Sample 2: FtsZ (5.0–12 μM) in 50 mM Tris-HCl, 500 mM KCl, 5 mM $MgCl_2$, and 1 mM GTP, pH 7.5 (Tris-KCl buffer), plus a GTP-regenerating system consisting of 1 unit/ml acetate kinase and 15 mM acetyl phosphate. Samples in Mes buffer were vitrified undiluted. At the highest concentrations in Tris-KCl assembly buffer with regenerating system, excess of protein made observations difficult, requiring polymer dilution (to 1.25 μM FtsZ) in prewarmed buffer just before being applied to the grid. Grids were observed in a model No. 1230 electron microscope (Jeol) operated at 100 kV and equipped with a liquid nitrogen specimen holder (Gatan). Micrographs from the hole areas, where the ice lacks any support film underneath, were recorded at a magnification of 40,000 under low dose conditions and different defocus on film (Kodak). Images were digitized using a Dimage Scan Multi Pro scanner (Konica-Minolta, Tokyo, Japan) at 2400 dpi corresponding to 0.265 nm/pixel. A few hundred images of filament segments were extracted from the micrographs with the boxer command from Eman (60) in two distinct data sets, and treated as single particles. Initial analysis of each data set was performed in 2D by reference-free classification of the data set in a collection of 2D averages using Eman 7.0.

This classification procedure revealed a collection of 2D averages for each data set. Classification and alignment within each group was further refined using the XMIPP suite of programs (61). Each average, with improved signal/noise ratio and built from a few tens of single images, was used to measure the FtsZ filament diameter. For this purpose, gray levels of the 2D averages at each pixel along several lines perpendicular to the longitudinal axis of the filament were plotted. The pixels considered to belong to the filaments were those whose gray level rose above the average level of the pixels of noise surrounding the filament. To calculate the final diameter of the filaments, the number of pixels measured was multiplied by 0.265 nm. The digitized cryo-EM images were also used to directly measure the thickness of the filaments using Image-J (image processing and analysis in Java; National Institutes of Health, Bethesda, MD). For this purpose, the micrographs were previously filtered using commands found in the Eman software to increase the signal/noise ratio. Filtered images were saved as .PNG files and then transferred to Image-J (National Institutes of Health). Thickness was measured by plotting the densities along lines that crossed perpendicular to the longitudinal axis of the filaments. Polymer contour lengths (L) and end-to-end distances (R) were also measured with Image-J (National Institutes of Health). Measurements obtained in pixels were then multiplied by 0.265 nm per pixel. The persistence length (P) of the polymers was estimated by classifying them in length classes, plotting the mean-squared end-to-end distance ($\langle R^2 \rangle$) versus L for classes with >5 R measurements and obtaining the best-fitting P employing Eqs. 9–11 from Rivetti et al. (62).

RESULTS

We have 1), investigated new methods for 2D crystallization of FtsZ protofilaments; 2), studied nucleated polymerization of FtsZ in solution and 3), polymers of FtsZ by cryo-EM on holey grids, which yielded a single protofilament width; and 4), formulated possible FtsZ polymerization models, including a mechanism for single-stranded nucleated assembly.

Adsorption-polymerization of an FtsZ construct from *M. jannaschii* on EM grids

Polymerization of the GTPase-inactive W319Y-His_6 mutant of FtsZ from *M. jannaschii* into sheet, previously assembled in solution (33), was optimized for formation of large 2D protein crystals on carbon-coated EM grids. Isothermal microdialysis of magnesium and nucleotide was employed to induce polymerization on grids floated on the sample solution. Different solution conditions screened included: pH (6.0–7.0), magnesium concentration (0–50 mM), ionic strength (0–1 M KCl), protein concentration (0.1–1 g L^{-1}), temperature (35–55°C), time (0–16 h), and nucleotide (GTP, GMPCPP, GDP; the sheet formation appeared more extensive with GDP). FtsZ sheet formed on the support (Fig. 1 *A*) in some cases spanned the support-free holes in holey grids (Fig. 1 *B*). These sheets had the same 5–7 nm projection width, double-filament structure (Fig. 1 *A*) described before (29,33) but were longer (up to tens of microns) and more abundant. Association of double filaments in a sheet is apparently facilitated by the histidine tag (33). Selected negative stain images gave computed diffractograms with spots up to 0.12 nm, but the projection maps failed to improve previous results (33). Cryo-EM diffractograms (Fig. 1 *C*), consistent with a 4.3 × 15.3 nm unit cell, did not yield meaningful projection maps because of the multilayer nature of most of the crystals. At this stage, these crystals have not yet been useful to improve the resolution of FtsZ filament EM models.

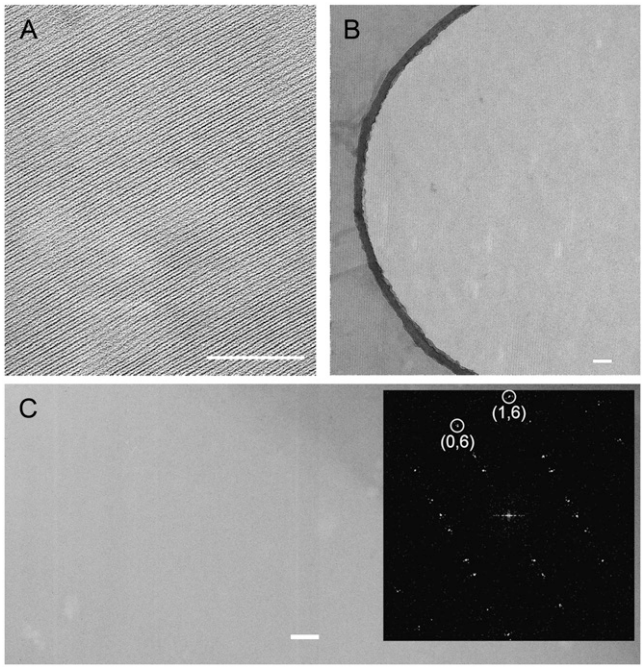

FIGURE 1 Polymerization of FtsZ from *M. jannaschii* (W319Y-His_6 mutant) on EM grids. Conditions: 50 mM Mes/KOH, 50 mM KCl, and 1 mM EDTA, pH 6.5, plus 12 mM $MgCl_2$ and 1 mM GDP, 45°C. (*A*) Negative stain image of an FtsZ sheet on a carbon-formvar grid. (*B*) Sheet spanning over a hole in a Quantifoil grid. (*C*) Cryo-EM image of a sheet sitting on carbon and computed diffractogram; spot (0,6) corresponds to a 2.50 nm spacing and (1,6) to 2.20 nm. Bars, 100 nm.

Nucleated polymerization of *E. coli* FtsZ in solution

Polymers of wild-type FtsZ from *M. jannaschii* have been shown to assemble in solution with a cooperative behavior after a nucleated polymerization mechanism (36). Since they have a marked tendency to form bundles (33,36), which might interfere with the observed energetics and hampers electron microscopy imaging of individual filaments, we employed through the rest of this study FtsZ from *E. coli*, which predominantly forms individual filaments. It was first necessary to determine the energetics of polymerization of *E. coli* FtsZ under the conditions of this study. FtsZ polymers assembled with GTP and magnesium in two different buffers at 30°C were quantified by high-speed pelleting. Buffers were 50 mM Mes-KOH, 50 mM KCl, 1 mM EDTA, 6 mM magnesium acetate, and 1 mM GTP, pH 6.5 (Mes buffer, similar to (19)) with or without a GTP-regenerating system, and 50 mM Tris-HCl, 500 mM KCl, 5 mM $MgCl_2$, and 1 mM GTP, pH 7.5, with the GTP-regenerating system consisting of 1 unit/ml acetate kinase and 15 mM acetyl

phosphate (27). FtsZ polymerization takes place above a defined critical concentration, $C_r = 0.88 \pm 0.25$ μM in Mes buffer and $C_r = 1.57 \pm 0.05$ μM in Tris-KCl buffer (Fig. 2, *A* and *B*), indicating that FtsZ assembles with a nucleus. Slopes of these plots are 0.80 with GTP excess and 0.90–0.99 with the regenerating system, indicating that most protein is active and that polymers are quantitatively sedimented. Interestingly, circular dichroism spectra of unassembled and polymerized FtsZ were very similar (Fig. 2 *C*), suggesting very small changes in the average secondary structure of the native protein upon assembly. Polymers formed using 1–12 μM FtsZ were observed by negative stain EM (Fig. 2, *D* and *E*). Filaments of ~4 and ~9 nm widths were observed in both buffer systems; this could be due to the presence of single and double FtsZ filaments or correspond to different projections of double protofilaments. At 1.2–1.7 μM FtsZ, close to the C_r value in Tris-KCl buffer, the polymers observed were predominantly individual filaments ~4 nm wide, of different lengths (Fig. 2 *D*). When the FtsZ concentration was increased above 1.7 μM, the polymers started to bundle and ~9-nm wide filaments appeared, while single filaments were still observed (Fig. 2 *E*). Below 1 μM, no polymers were found. Similar results were obtained in Mes buffer (not shown).

Cryo-EM of *E. coli* FtsZ filament solutions on holey grids

FtsZ polymers were studied by cryo-EM, allowing direct molecular visualization without staining, fixation, or adsorption to a support (63). FtsZ samples were prepared in the two different buffers (see above) at different FtsZ concentrations. Visual inspection of micrographs revealed FtsZ polymers of various lengths and curvatures, very similar in structure under each solution conditions (Fig. 3), so all the images obtained could be indistinctly analyzed for the purpose of measuring filament width. Apparent sample differences in filament curvature (Fig. 3, *A* and *C*) may relate to the different experimental conditions and polymer concentrations. Filaments of two apparent diameters were observed, labeled thin and thick henceforth. A few hundred images of thin and thick filaments segments were extracted from the micrographs and treated as single particles (Fig. 4, *A* and *B*) to finally obtain a few averages from the initial data. Each average was used to measure the filament diameter, from plots of the gray levels of the 2D averages at each pixel along several lines perpendicular to the longitudinal filament axis (Fig. 4, *C* and *D*). The filament diameter values turned out to be 5.6 $\pm$ 0.5 nm and 4.1 $\pm$ 0.5 nm (average $\pm$ standard error). As our classification may be a simplification of different lateral projections of an FtsZ protofilament, filament thickness was approximately measured directly from cryo-electron micrographs (Fig. 4 *E*, including the single circle found) with Image-J. This program displays a two-dimensional graph of the intensities of pixels along a line within the image, showing a relatively wide distribution centered between 5–6 nm (5.4 nm $\pm$ 0.9 nm) (Fig. 4 *F*); still, a very small proportion of these measurements were consistent with double filaments, but this could also be a result of experimental error in the measurement method used. The

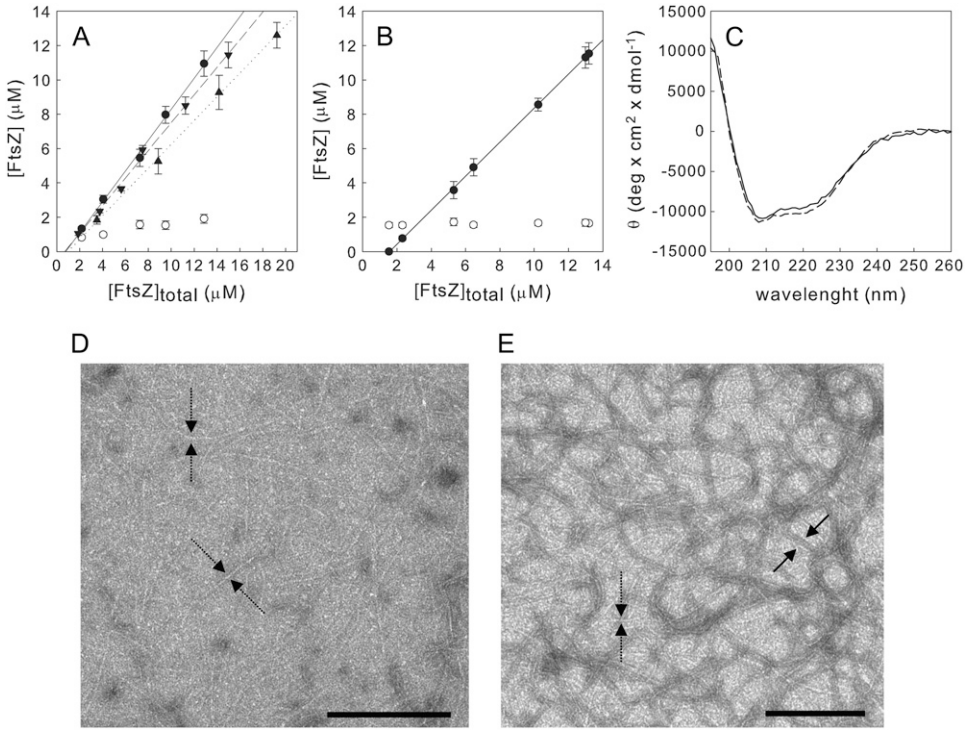

FIGURE 2 Polymerization of *E. coli* FtsZ. (*A*) Sedimentation measurements of polymers formed in Mes assembly buffer, pH 6.5, with 1 mM GTP (▲), 4 mM GTP (▼), or 1 mM GTP plus a GTP-regenerating system (●). (*B*) Measurements in Tris-KCl buffer, pH 7.5, with 1 mM GTP and the GTP-regenerating system. Void symbols are FtsZ concentrations in the supernatant. (*C*) Circular dichroism spectra of 12 μM unassembled FtsZ (*solid line*, minus GTP) and polymerized FtsZ (*dash line*, with 0.5 mM GTP) in Tris-KCl buffer with GTP-regenerating system (similar results were obtained in Mes assembly buffer with 0 and 4 mM GTP). (*D* and *E*) Electron micrographs of the FtsZ polymers formed in Tris-KCl buffer with the GTP-regenerating system at 1.5 μM (*D*) and 12.5 μM FtsZ (*E*). Bars are 200 nm. Arrows mark filament bundles and dotted arrows mark single filaments.

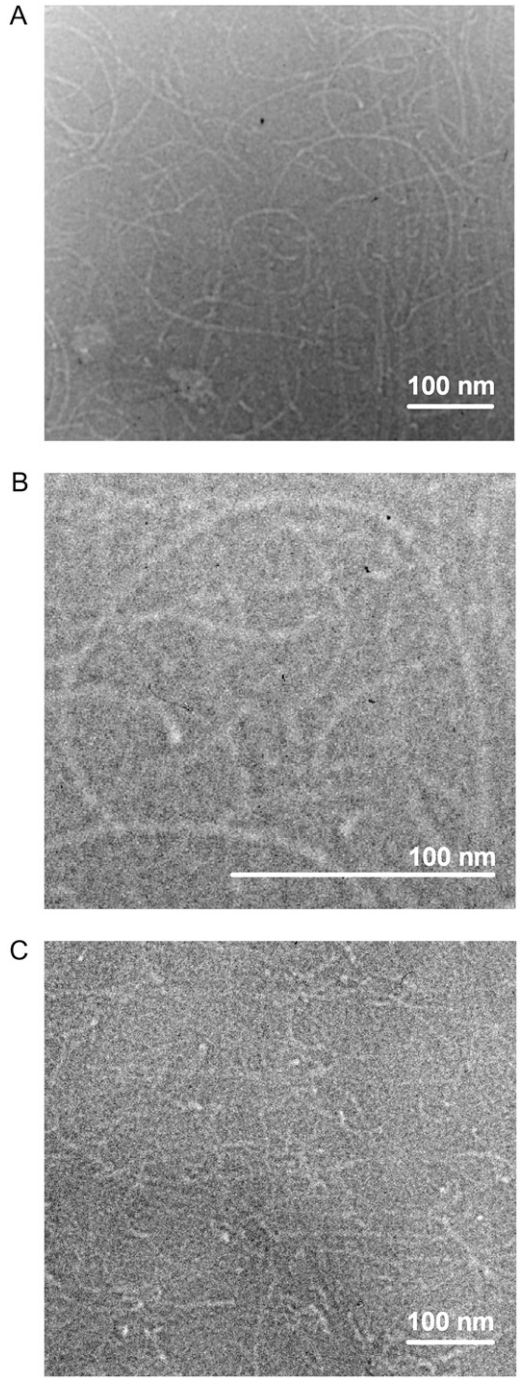

FIGURE 3 Cryo-EM images of FtsZ polymers on holey grids. (*A*) FtsZ (12.5 μM) in Mes assembly buffer pH 6.5, 1 mM GTP (the sample was frozen before 1 min after GTP addition and light scattering controls indicated that the polymers remain in the solution for >10 min); (*B*) enlargement of the central zone of image *A*. (*C*) FtsZ (5 μM) assembled in Tris-KCl assembly buffer pH 7.5, 1 mM GTP plus a GTP-regenerating system. Bars are 100 nm.

cryo-EM width measurements are collectively compatible with single FtsZ protofilaments (4.2–5.7 nm, from the maximum and minimum projection widths of an FtsZ dimer (8); 4.4 nm from negatively stained double filaments (33); ~4.7 nm from a pseudoatomic model of FtsZ double filament (29)), but are incompatible with double FtsZ protofilaments (8.4–11.4 nm).

The filament lengths in Mes buffer had a wide asymmetric distribution (Fig. 4 *G*) with an average length $\langle L \rangle$ of 196 nm (standard deviation, 126 nm). The average end-to-end distance $\langle R \rangle$ was 134 nm (standard deviation, 63 nm). To estimate the flexural rigidity of FtsZ filaments in these samples, $\langle R^2 \rangle$ was plotted versus L and a best fitting persistence length P-value of 54 $\pm$ 2 nm was determined (Fig. 4 *H*), assuming 2D thermal bending of the filaments (62) in the thin sample layer immediately before freezing. Note that if the bending was three-dimensional (62) the corresponding P-value would be 162 $\pm$ 6 nm, slightly below $\langle L \rangle$.

Model of nucleated linear polymerization with monomer conformational switching

A plausible mechanism for apparently cooperative single-stranded polymerization of FtsZ was not found before (26), but this has been suggested possible if a conformational change that increases the affinity of the next monomer to bind is taken into account (4). A simple model for nucleated linear polymerization is formulated below, explaining the results of this study, as well as purified FtsZ assembly in solution. Other equilibrium models for the polymerization of cell division protein FtsZ, formulated in Supplementary Material, facilitate analysis of previous results and models from the literature. These include double-stranded filament, polymerization coupled to surface adsorption, or membrane attachment and single-stranded filament with cyclic end-product.

Let us consider an indefinite linear self-association linked to an activation structural change of the monomer (Fig. 5). The free energy change for dimer formation is $\Delta G(2) = 2\Delta Gc_1 + \Delta Ga_1$, and free energy change of further elongation steps is $\Delta G(n > 2) = \Delta Gc_1 + \Delta Ga_1$. It follows that for an unfavorable monomer structural change ($\Delta Gc_1 > 0$), $\Delta G(n > 2) < \Delta G(2)$, polymerization appears cooperative with a dimer nucleus. Linkage of polar linear association and structural change implies allosteric communication between the two different association ends of each monomer (Fig. 5). Consider for simplicity the isomerization of isolated monomers before their proper association; naming C_1 the inactive monomers, S_i the active species, and c_1 and s_i their respective concentrations, the equilibria involved are

$$C_1 \rightleftharpoons S_1 \quad \text{where} \quad s_1 = K_c c_1, \tag{1}$$

$$2\,S_1 \rightleftharpoons S_2 \quad \text{where} \quad s_2 = K_c^2 K_a c_1^2, \tag{2}$$

$$S_2 + S \rightleftharpoons S_3 \quad \text{where} \quad s_3 = K_c^3 K_a^2 c_1^3, \tag{3}$$

$$S_{i-1} + S \rightleftharpoons S_i \quad \text{where} \quad s_i = K_a^{-1}(K_c K_a c_1)^i. \tag{4}$$

By mass conservation, the total protein concentration, C_0, is

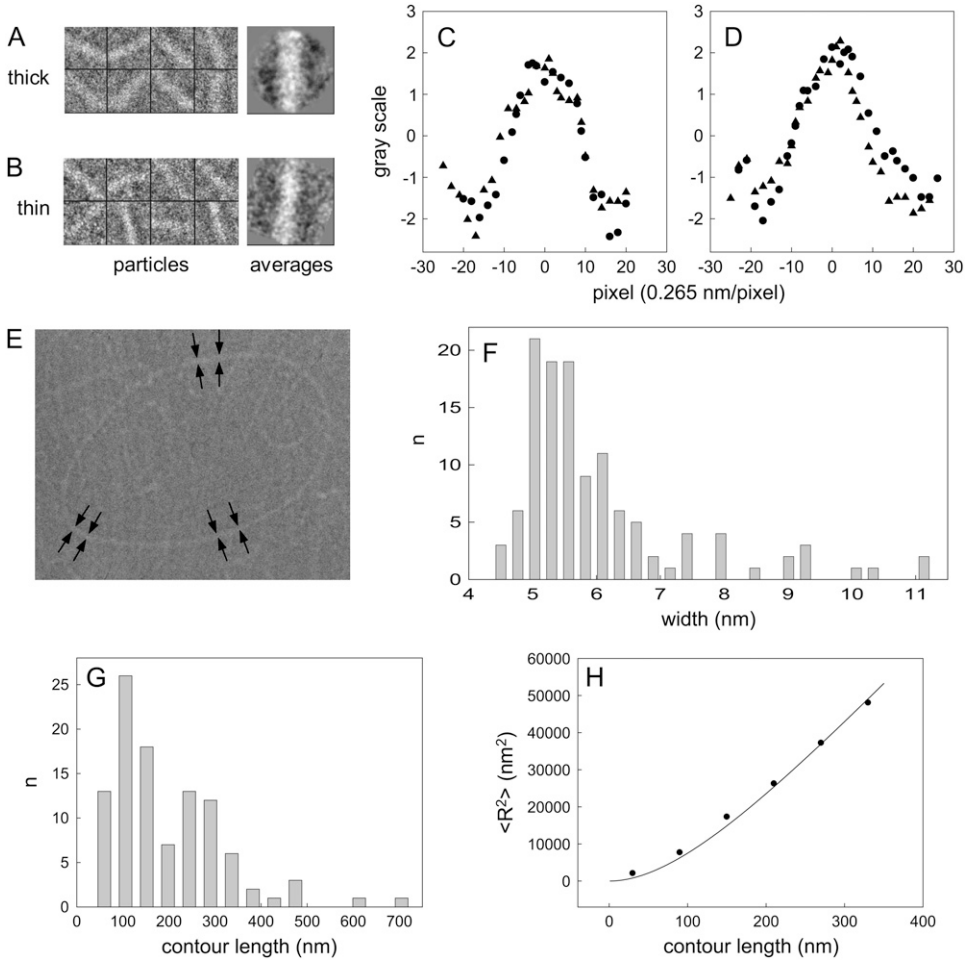

FIGURE 4 FtsZ filament width determined by cryo-EM. (*A* and *B*) A gallery of representative thin and thick filaments boxed out from the original cryo-electron micrographs. Right panels show the 2D average derived after classification, alignment and averaging using Eman and XMIPP for each data set. (*C* and *D*) Density profiles perpendicular to the longitudinal axis of the average images corresponding to thick (*C*) and thin (*D*) filaments. Measurements were made in two zones for each average filament. (*E*) An area from a cryo-electron micrograph of FtsZ polymers. Arrows over the filament indicate positions used to measure the thickness with the Image-J program. One-hundred-and-six measurements were made of more than 10 different areas from several micrographs obtained under different experimental conditions. (*F*) Number of measurements (*y* axis) for each width (*x* axis). (*G*) Filament length distribution. (*H*) Measurements of mean squared end-to-end distance versus filament length. The solid line corresponds to the best-fitted persistence length values (Experimental Methods) given in the text.

$$C_0 = c_1 + \sum_1^\infty iS_i = c_1 + K\mathrm{a}^{-1} \sum_1^\infty \mathrm{i}(K_\mathrm{c}\, K_\mathrm{a}\, c_1)^\mathrm{i}. \qquad (5)$$

For $K_\mathrm{c}\, K_\mathrm{a}\, c_1 < 1$, the power series in Eq. 5 converges to

$$C_0 = c_1 + K_\mathrm{c} c_1/(1 - K_\mathrm{c} K_\mathrm{a} c_1)^2, \qquad (6)$$

which is identical to Oosawa's equation for condensation polymerization (44),

$$C_0 = c_1 + \sigma c_1/(1 - K_\mathrm{h} c_1)^2, \qquad (7)$$

setting the cooperativity parameter $\sigma = K_\mathrm{c}$ and the helical polymer elongation constant $K_\mathrm{h} = K_\mathrm{c}\, K_\mathrm{a}$, where $K_\mathrm{h} \approx C_\mathrm{r}^{-1}$. Therefore, this self-switching model is seemingly indistinguishable from a typical multistranded condensation polymerization. Note that, in Eq. 7, $\sigma = \gamma\,(K/K_\mathrm{h})^{\mathrm{n}-1}$, where K is the linear association constant and γ the equilibrium constant of deformation of linear into helical n-mer (44); $\gamma < 1$ is another way to introduce a nucleation energy difference independent of multiple contacts. A linear polymer does not nucleate in the absence of other features such as internal energy changes (52). The concept of self-switching assembly was actually anticipated by Caspar (39,40), after Penrose's proposal of mechanical self-reproducing machines (64) and the autocatalytic polymerization of flagellin (65). Caspar showed that self-controlled conformational switching can account for the nucleation energy difference and appear as cooperative, even for a linear structure, and proposed a regulatory role for this autosteric process (39,40).

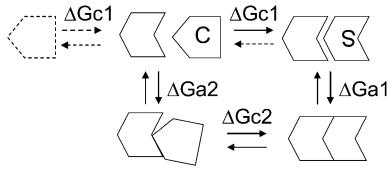

FIGURE 5 Scheme of indefinite linear protein self-association linked to an activation structural change. Shape *C* represents a ground-state monomer, and shape *S* represents a monomer activated for correct association. In pathway 1, structural change precedes association, whereas in pathway 2, association precedes structural change. It holds that $\Delta Gc_1 + \Delta Ga_1 = \Delta Ga_2 + \Delta Gc_2$. The linkage free energy is $\Delta G_\mathrm{link} = \Delta Gc_2\text{-}\Delta Gc_1 = \Delta Ga_1\text{-}\Delta Ga_2$. For $\Delta G_\mathrm{link} < 0$, structural change and association favor each other. The free energy of the structural change counts twice for dimerization but only once for further elongation steps. If $\Delta Gc_1 > 0$, the association becomes cooperative with a dimer nucleus.

DISCUSSION

Apparently cooperative FtsZ polymers are single-stranded and flexible

Cooperative behavior of FtsZ assembly (66) was supported by a number of other studies (4,26,33,36). Sedimentation assays in this and another study under same solution conditions (34) confirm GTP and magnesium-induced assembly of *E. coli* FtsZ as an abrupt process involving all the protein in excess of a critical concentration, which is incompatible with simple linear polymerization (44). The important questions are: 1), what FtsZ polymers are formed in solution, whether single-, multistranded, or other; 2), whether their geometry can be made compatible with cooperative behavior; and 3), how the polymerization of isolated FtsZ relates to its in vivo assembly in the FtsZ ring.

Negative-stain EM images show *E. coli* FtsZ polymers one- and two-protofilament wide (Fig. 2) in the critical concentration region, with the proportion of pairs and bundles apparently increasing with protein concentration. Image analysis of similar *E. coli* FtsZ polymers and polymers of *M. jannaschii* FtsZ showed two side-by-side protofilaments, with the tubulin-like 4-nm axial spacing between FtsZ monomers (33). However, due to reports of single versus double FtsZ filaments (see Introduction) and the possibility that adsorption to the grid may modify FtsZ protofilament association, minimum possible sample perturbation was desirable. FtsZ polymers assembled under two typical solution conditions were fast-frozen on holey grids and observed in vitreous ice. Cryo-EM images show filaments with 5–6 nm width measurements (Figs. 3 and 4), compatible only with single FtsZ protofilaments. These filaments have variable lengths distributed around an average of ~200 nm or 46 FtsZ monomers (based on 4.3 nm per monomer; (33)). They appear quite flexible, with a persistence length comprised between 13 and 38 FtsZ monomers, although we cannot rule out mechanical perturbation of the polymers by sample blotting before vitrification. The lower limit of the estimated persistence length of FtsZ polymers practically coincides with the 50-nm persistence length of DNA (62). This estimated persistence length of FtsZ filaments, in Mes buffer pH 6.5 with 1 mM GTP, is two and five orders-of-magnitude smaller than typical persistence lengths of actin filaments and microtubules, respectively (67). Future measurements of FtsZ polymers length and flexibility as functions of GTP hydrolysis and solution variables might give insight into their disassembly mechanism.

FtsZ polymerization with adsorption on carbon and mica supports

It is possible that previously studied double-stranded FtsZ filaments (29,33) may not form in the solution, after a double-stranded polymerization model (Supplementary Material, Fig. S6). Instead, they may form on the EM grid due to protofilament association on the carbon support, according to models of polymerization coupled to adsorption (Supplementary Material, Fig. S7). Therefore the double filament observations are real but cannot be employed to explain the cooperative behavior of FtsZ assembly in solution (36). Observation of one and two protofilament widths in negatively stained FtsZ polymers and only one protofilament in cryo-EM in this study may similarly be due to protofilament accretion on the carbon support. An extreme case of adsorption-polymerization is the enhanced crystallization of mutant FtsZ from *M. jannaschii* on carbon-coated EM grids (Fig. 1). Ordered deposition of thermophilic FtsZ onto solid supports has potential bionanotechnological applications (68,69). Other results and models from the literature and a suitable mechanism for the nucleated polymerization of single protofilaments of *E. coli* FtsZ are discussed below.

Employing STEM and low FtsZ concentrations on thin carbon films, Romberg et al. (25) measured mass values of 40 ± 5 kDa per 4-nm lengths of *E. coli* FtsZ filaments, corresponding only to single protofilaments. By negative stain EM they found 4.6-nm-wide filaments at low protein concentrations, which formed pairs or bundles at higher protein concentration and longer time. Our cryo-EM width measurements, in agreement with the STEM results, overcome the concern that protofilament adsorption on the STEM support might have dissociated double-stranded filaments from the solution (Supplementary Material, Figs. S6 and S7). AFM of mica-adsorbed *E. coli* FtsZ polymers also showed single dynamic protofilaments, 4-nm thick and 4.8-nm wide at half-thickness (28).

Preferential cyclization does not explain cooperative FtsZ assembly with GTP

Gonzalez et al. (27) observed a narrow fast sedimenting boundary (~12 S) in polymerizing FtsZ solutions, together with some protofilament rings in negative stain and AFM, and proposed preferential cyclization to qualitatively explain how a single FtsZ protofilament could be cooperative. Such a cooperative single protofilament with a cyclic end product would require a significantly favorable closure free energy change (Supplementary Material, Fig. S9), implying that practically all polymers in solution are closed. However, FtsZ polymers are generally observed by EM to be predominantly open, even in that study (27). Application of preferential cyclization to FtsZ assembly is also contradicted by our cryo-EM images under identical solution conditions (Figs. 3 and 4) and by polymerization kinetics (2,26). In addition, with increasing protein concentrations, preferential cyclization implies bimodal sedimentation profiles corresponding to a nearly constant monomer concentration and a linearly increasing ring concentration (Supplementary Material, Fig. S9). However, neither was such concentration dependence quantified (actually, the monomer peak seems to disappear), nor were the sedimentation profiles numerically

fitted by association models (27). On the other hand, abundant cyclic protofilaments ~100 nm in diameter form with GDP-$AlFl_X$ (28,70), which might be examined for the presence of a ~12 S peak. The origin of the ~12 S sedimenting peak in FtsZ solutions with GTP should be reinvestigated, as well as the biological relevance of purified FtsZ rings.

Self-switching assembly of a single FtsZ protofilament with a dimer nucleus

Chen and co-workers studied the kinetics of GTP-induced polymerization of a L68W mutant of *E. coli* FtsZ with tryptophan fluorescence and stopped-flow (26), as well as fluorescently labeled *E. coli* FtsZ with resonance energy transfer (17). Sigmoidal time-courses, including a lag time, were globally fitted by a reaction mechanism consisting of monomer activation and a weak dimer nucleation followed by elongation. Single protofilaments were observed by negative stain as with STEM previously (25), but a plausible model of how a one-subunit thick filament could assemble with a cooperative behavior was not proposed (26). Very recently, they have reported the slow assembly of FtsZ from *Mycobacterium tuberculosis* into one- or two-stranded negatively stained polymers depending on pH. However, the kinetics could be fitted by the same scheme with a dimer nucleus in both cases, leading to the conclusion that the observed two-stranded assembly of *M. tuberculosis* FtsZ was apparently not related to their hypothetical dimer nucleus but may be a secondary association event (71).

This study shows that nucleated *E. coli* FtsZ assembly forms single-stranded filaments (cryo-EM Results) and that this can be explained only, among possible models, by a simple mechanism of protofilament polymerization with monomer activation, which can behave cooperatively with a dimer nucleus (see Model of Nucleated Linear Polymerization with Monomer Conformational Switching, Fig. 1, and Discussion above). This implies counting the unfavorable free energy change of the monomer switch, once for each elongation step but twice for dimerization. The possibility that FtsZ polymerization may involve this type of process has been suggested in two recent reviews (4,72). Determination of the reaction scheme, whether activation precedes or follows elongation, and the free energy change of monomer switching will require further kinetic analysis.

Self-switching in protein assembly systems

Self-controlled switching in protein assembly (39,40) involves an energy difference between ground state and activated monomers, which hampers nucleation but is not dependent on multiple contacts, such as it occurs in crystal nucleation. This concept is currently essential for understanding the regulation of functional protein assembly systems, as well as amyloid formation. It implies very simple isomerization-association reaction schemes resulting in a critical concentration (see Model). The model is formally equivalent to replacing the free energy change of lateral interaction by the monomer isomerization free energy change. In multistranded cytoskeletal protein polymers, such as tubulin, actin, MreB, or flagellin, each subunit added to the polymer makes several intermolecular contacts. The DNA-binding protein RecA crystallized as packed single-stranded helical polymers, and the active nucleoprotein filaments of RecA-like ATP-bound proteins cooperatively polymerize on DNA (73,74). RecA can form structurally similar polymers without DNA in high salt and D_20 (75), although we have not found reports of a critical concentration for RecA self-polymerization. The crystal structure of the replication initiator DnaA bound to the ATP analog AMP-PCP has revealed a single-stranded helical filament, and ATP binding allows DnaA to switch from a monomeric state into a large oligomeric nucleoprotein complex (76). In many of these cases, protein subunits typically form either multiple stranded polymers or single protein filaments bound to DNA. Therefore quantifying the contribution to cooperative polymerization of monomer switching among the several intermolecular contacts made by each subunit is difficult. In fact, nucleated protein polymerization systems have generally been simply explained by multiple contacts of rigid subunits, neglecting self-switching. The nucleated single-stranded FtsZ assembly obviates this difficulty, since there is only one intermolecular contact formed per added subunit.

Yeast prion amyloid fibrils propagate by self-replication. Ure2p and Sup35p fibrils have nearly one prion molecule per 0.47 nm repeat period, which is compatible with a single-stranded structure (77,78), and Sup35p grows according to a linear nucleation and monomer addition model (79). These and other amyloids are dramatic cases of templated structural switching from native protein monomers into cross-β spines (80,81), with profound pathological implications. In the case of FtsZ, a native structure is maintained and the structural switch serves the regulatory purpose of assembly and disassembly. At this point we are not aware of any other protein which self-assembles under physiological solution conditions into a nucleated single-stranded filament in a functionally relevant process.

The FtsZ and tubulin activation/depolymerization switches

The conclusion that, for nucleated assembly of an FtsZ protofilament, the activation equilibrium of the isolated monomer must be unfavorable (see Model and Fig. 5) supports the proposal, made on totally independent grounds, that unassembled FtsZ and tubulin exist predominantly in inactive states which isomerizes into the active states by polymerization-driven structural changes (14), instead of undergoing nucleotide-dependent structural changes when unassembled (15). The inactive species C and the active species S in Eqs. 1–4 are

immediately identified with the so-called curved and straight states, respectively (14). Binding of the GTP γ-phosphate lowers the free energy difference between these states, allowing the flexibility required to adopt the active conformation driven by the polymer contacts (14). This has been exemplified by a two-state transition, but depending on the size of the activation energy barrier, a continuum of intermediate structures could exist with different nucleotide binding affinities. In the case of tubulin the lateral contacts in a microtubule overcome the tendency of flexible protofilaments to curve (Fig. 3 in (14)), whereas in the case of a single FtsZ protofilament there are only axial contacts but no lateral contacts to straighten the protofilaments (Fig. 5) which adopt variable curvatures (Fig. 3). The strain induced by nucleotide hydrolysis at an association interface should directly cause FtsZ protofilament fragmentation, since it cannot be compensated by additional contacts in a metastable polymer lattice such as in microtubules.

The nature of the structural flexibility changes coupled to FtsZ assembly is not known; this will require determining the structure of an FtsZ filament. There should be changes both at the polymerization interfaces and within the monomers. These changes switching between the active and inactive states could be significant structural changes or flexibility changes with very small structural displacements. On one hand, the presence or absence of the nucleotide γ-phosphate at the polymerization interface modifies the association affinity and the gross structure of polymers of FtsZ from *M. jannaschii* (13,26). On the other hand, nucleated assembly of single-stranded polymers of *E. coli* FtsZ (this study) requires allosteric communication between the top and bottom monomer association interfaces (Fig. 5), which implies some internal monomer structural change. One possibility is that this information transfer might be provided by an observed displacement of tubulin core helix H7, spanning from the bottom to the top association interfaces of a monomer (82). We suggested that a similar displacement might take part in a conserved activation switch in FtsZ (see Figs. 1 and 2 in (14)). Specifically, binding of the preceding FtsZ monomer might pull from loop T7-helix H7 at the bottom interface, generating the active conformation at the top interface and thus facilitating the binding of the next FtsZ monomer. A very recent structural comparison of 14 different FtsZ monomer structures has not favored this tubulin-like mechanism for FtsZ, but supported an FtsZ switch driven by lateral protofilament association (83).

FtsZ appears to be a primitive nucleated linear assembly machine. It has been suggested that FtsZ and tubulin polymerization evolved by GTP-binding domain fusion with the C-terminal GTPase activating domain (both previously individual interacting proteins) and that the resulting fusion protein associated into a linear polymer based on domain interactions (8). Tubulin acquisition of new surface loop sequences conferred the ability to laterally associate protofilaments into eukaryotic microtubules (the lateral accretion cooperating with the monomer activation switch; (14)), which in turn generated folding problems requiring the concourse of the chaperonin CCT (11,12).

Geometry of FtsZ polymers in vitro and in vivo

Given the polymorphic assembly products of purified FtsZ, the effects of partner proteins and of cytosolic macromolecular crowding, the dynamics of the Z-ring and the subcellular FtsZ images (2,4,5,16,33,34), any type of structures may have been expected for FtsZ polymers in vivo. The structure of the bacterial cytokinetic ring, which has eluded visualization for 15 years, is being unveiled. Employing cryo-EM of unfixed hydrated vitreous sections, Zuber et al. (37) observed, at the constriction ring of *Enterococcus gallinarum*, 3–6 nm thick cytoplasmic filaments, spaced 5–7 nm, which may form layers or rings 7–12 nm below the plasma membrane; these are thought to be FtsZ polymers. A 7–12 nm distance is within the span of ZipA, a protein linking the FtsZ filaments to the plasma membrane in *E. coli* (84), a bacterium in which the FtsZ filaments have not been visualized by EM. An electron cryotomography study of the cytoskeleton of *Caulobacter crescentus* revealed, among other fibers, bundles of ~5-nm-thick filaments packed 11 nm apart, thought to be FtsZ (38). Very recently the Jensen laboratory has reported the structure of the *C. crescentus* FtsZ ring, actually consisting of a few short (~100 nm) FtsZ filaments ~5 nm in diameter, below the plasma membrane near the division site, and suggested that these FtsZ polymers generate the force that constricts the membrane through iterative cycles of GTP hydrolysis, depolymerization and repolymerization. A full turn of the discontinuous ring was not visualized due to the missing information in the tomograms, and the current resolution was insufficient to reveal the subunit repeat and to rule out the possibility that the filaments were double (85). The ~5-nm width observed so far for the putative membrane-attached FtsZ filaments from these two living bacterial cells would be compatible with the Z-ring being formed by single protofilament FtsZ polymers such as those observed in vitro in this study. However, both the confirmation and extension of these observations of FtsZ polymers to other bacteria, and the extent to which nucleated self-assembly of single FtsZ protofilaments may function in cells, await further investigation.

SUPPLEMENTARY MATERIAL

To view all of the supplemental files associated with this article, visit www.biophysj.org.

We thank Drs. D. L. D. Caspar and J. F. Díaz for discussions on early versions of the manuscript.

This work was supported in part by grants No. MEC BFU 2005-00505/BMC (to J.M.A.), No. SAF 2005-00775 (to O.L.), No. BFU 2004-00232/BMC (to J.M.V.), grant No. CAM S-BIO-0214-2006 (to O.L., J.M.A.), and a CSIC-I3P contract (to S.H.).

REFERENCES

1. Bi, E., and J. Lutkenhaus. 1991. FtsZ ring structure associated with division in *Escherichia coli*. *Nature*. 354:161–164.
2. Margolin, W. 2005. FtsZ and the division of prokaryotic cells and organelles. *Nat. Rev. Mol. Cell Biol.* 6:862–871.
3. Rothfield, L., A. Taghbalout, and Y. L. Shih. 2005. Spatial control of bacterial division-site placement. *Nat. Rev. Microbiol.* 3:959–968.
4. Michie, K. A., and J. Löwe. 2006. Dynamic filaments of the bacterial cytoskeleton. *Annu. Rev. Biochem.* 75:467–492.
5. Vicente, M., and A. I. Rico. 2006. The order of the ring: assembly of *Escherichia coli* cell division components. *Mol. Microbiol.* 61:5–8.
6. Lutkenhaus, J. 2007. Assembly dynamics of the bacterial MinCDE system and spatial regulation of the Z ring. *Annu. Rev. Biochem.* n press.
7. Nogales, E., K. H. Downing, L. A. Amos, and J. Lowe. 1998. Tubulin and FtsZ form a distinct family of GTPases. *Nat. Struct. Biol.* 5:451–458.
8. Oliva, M. A., S. C. Cordell, and J. Löwe. 2004. Structural insights into FtsZ protofilament formation. *Nat. Struct. Mol. Biol.* 11:1243–1250.
9. Nogales, E., M. Whittaker, R. A. Milligan, and K. H. Downing. 1999. High-resolution model of the microtubule. *Cell.* 96:79–88.
10. Llorca, O., J. Martin-Benito, P. Gomez-Puertas, M. Ritco-Vonsovici, K. R. Willison, J. L. Carrascosa, and J. M. Valpuesta. 2001. Analysis of the interaction between the eukaryotic chaperonin CCT and its substrates actin and tubulin. *J. Struct. Biol.* 135:205–218.
11. Andreu, J. M., M. A. Oliva, and O. Monasterio. 2002. Reversible unfolding of FtsZ cell division proteins from archaea and bacteria. Comparison with eukaryotic tubulin folding and assembly. *J. Biol. Chem.* 277:43262–43270.
12. Bertrand, S., I. Barthelemy, M. A. Oliva, J. L. Carrascosa, J. M. Andreu, and J. M. Valpuesta. 2005. Folding, stability and polymerization properties of FtsZ chimeras with inserted tubulin loops involved in the interaction with the cytosolic chaperonin CCT and in microtubule formation. *J. Mol. Biol.* 346:319–330.
13. Huecas, S., and J. M. Andreu. 2004. Polymerization of nucleotide-free, GDP- and GTP-bound cell division protein FtsZ: GDP makes the difference. *FEBS Lett.* 569:43–48.
14. Buey, R. M., J. F. Diaz, and J. M. Andreu. 2006. The nucleotide switch of tubulin and microtubule assembly: a polymerization-driven structural change. *Biochemistry.* 45:5933–5938.
15. Nogales, E., and H. W. Wang. 2006. Structural mechanisms underlying nucleotide-dependent self-assembly of tubulin and its relatives. *Curr. Opin. Struct. Biol.* 16:1–9.
16. Stricker, J., P. Maddox, E. D. Salmon, and H. P. Erickson. 2002. Rapid assembly dynamics of the *Escherichia coli* FtsZ-ring demonstrated by fluorescence recovery after photobleaching. *Proc. Natl. Acad. Sci. USA.* 99:3171–3175.
17. Chen, Y., and H. P. Erickson. 2005. Rapid in vitro assembly dynamics and subunit turnover of FtsZ demonstrated by fluorescence resonance energy transfer. *J. Biol. Chem.* 280:22549–22554.
18. Mingorance, J., S. Rueda, P. Gomez-Puertas, A. Valencia, and M. Vicente. 2001. *Escherichia coli* FtsZ polymers contain mostly GTP and have a high nucleotide turnover. *Mol. Microbiol.* 41:83–91.
19. Romberg, L., and T. J. Mitchison. 2004. Rate-limiting guanosine 5′-triphosphate hydrolysis during nucleotide turnover by FtsZ, a prokaryotic tubulin homologue involved in bacterial cell division. *Biochemistry.* 43:282–288.
20. Burbank, K. S., and T. J. Mitchison. 2006. Microtubule dynamic instability. *Curr. Biol.* 16:R516–R517.
21. Ben-Yehuda, S., and R. Losick. 2002. Asymmetric cell division in *B. subtilis* involves a spiral-like intermediate of the cytokinetic protein FtsZ. *Cell.* 109:257–266.
22. Thanedar, S., and W. Margolin. 2004. FtsZ exhibits rapid movement and oscillation waves in helix-like patterns in *Escherichia coli*. *Curr. Biol.* 14:1167–1173.
23. Mukherjee, A., and J. Lutkenhaus. 1994. Guanine nucleotide-dependent assembly of FtsZ into filaments. *J. Bacteriol.* 176:2754–2758.
24. Erickson, H. P., D. W. Taylor, K. A. Taylor, and D. Bramhill. 1996. Bacterial cell division protein FtsZ assembles into protofilament sheets and minirings, structural homologs of tubulin polymers. *Proc. Natl. Acad. Sci. USA.* 93:519–523.
25. Romberg, L., M. Simon, and H. P. Erickson. 2001. Polymerization of FtsZ, a bacterial homolog of tubulin. Is assembly cooperative? *J. Biol. Chem.* 276:11743–11753.
26. Chen, Y., K. Bjornson, S. D. Redick, and H. P. Erickson. 2005. A rapid fluorescence assay for FtsZ assembly indicates cooperative assembly with a dimer nucleus. *Biophys. J.* 88:505–514.
27. Gonzalez, J. M., M. Velez, M. Jimenez, C. Alfonso, P. Schuck, J. Mingorance, M. Vicente, A. P. Minton, and G. Rivas. 2005. Cooperative behavior of *Escherichia coli* cell-division protein FtsZ assembly involves the preferential cyclization of long single-stranded fibrils. *Proc. Natl. Acad. Sci. USA.* 102:1895–1900.
28. Mingorance, J., M. Tadros, M. Vicente, J. M. Gonzalez, G. Rivas, and M. Velez. 2005. Visualization of single *Escherichia coli* FtsZ filament dynamics with atomic force microscopy. *J. Biol. Chem.* 280:20909–20914.
29. Löwe, J., and L. A. Amos. 1999. Tubulinlike protofilaments in Ca^{2+}-induced FtsZ sheets. *EMBO J.* 18:2364–2371.
30. Lu, C., J. Stricker, and H. P. Erickson. 1998. FtsZ from *Escherichia coli*, *Azotobacter vinelandii*, and *Thermotoga maritima*—quantitation, GTP hydrolysis, and assembly. *Cell Motil. Cytoskeleton.* 40:71–86.
31. Mukherjee, A., and J. Lutkenhaus. 1999. Analysis of FtsZ assembly by light scattering and determination of the role of divalent metal cations. *J. Bacteriol.* 181:823–832.
32. Rivas, G., A. Lopez, J. Mingorance, M. J. Ferrandiz, S. Zorrilla, A. P. Minton, M. Vicente, and J. M. Andreu. 2000. Magnesium-induced linear self-association of the FtsZ bacterial cell division protein monomer. The primary steps for FtsZ assembly. *J. Biol. Chem.* 275:11740–11749.
33. Oliva, M. A., S. Huecas, J. M. Palacios, J. Martin-Benito, J. M. Valpuesta, and J. M. Andreu. 2003. Assembly of archaeal cell division protein FtsZ and a GTPase-inactive mutant into double-stranded filaments. *J. Biol. Chem.* 278:33562–33570.
34. Gonzalez, J. M., M. Jimenez, M. Velez, J. Mingorance, J. M. Andreu, M. Vicente, and G. Rivas. 2003. Essential cell division protein FtsZ assembles into one monomer-thick ribbons under conditions resembling the crowded intracellular environment. *J. Biol. Chem.* 278:37664–37671.
35. Thanbichler, M., and L. Shapiro. 2006. MipZ, a spatial regulator coordinating chromosome segregation with cell division in *Caulobacter*. *Cell.* 126:147–162.
36. Huecas, S., and J. M. Andreu. 2003. Energetics of the cooperative assembly of cell division protein FtsZ and the nucleotide hydrolysis switch. *J. Biol. Chem.* 278:46146–46154.
37. Zuber, B., M. Haenni, T. Ribeiro, K. Minnig, F. Lopes, P. Moreillon, and J. Dubochet. 2006. Granular layer in the periplasmic space of Gram-positive bacteria and fine structures of *Enterococcus gallinarum* and *Streptococcus gordonii* septa revealed by cryo-electron microscopy of vitreous sections. *J. Bacteriol.* 188:6652–6660.
38. Briegel, A., D. P. Dias, Z. Li, R. B. Jensen, A. S. Frangakis, and G. J. Jensen. 2006. Multiple large filament bundles observed in *Caulobacter crescentus* by electron cryotomography. *Mol. Microbiol.* 62:5–14.
39. Caspar, D. L., and A. Klug. 1962. Physical principles in the construction of regular viruses. *Cold Spring Harb. Symp. Quant. Biol.* 28:1–24.
40. Caspar, D. L. 1980. Movement and self-control in protein assemblies. Quasi-equivalence revisited. *Biophys. J.* 32:103–138.
41. Makowski, L. 1998. An unreasonable man in a quasi-equivalent world. *Biophys. J.* 74:534–536.
42. Crick, F. H., and J. D. Watson. 1956. Structure of small viruses. *Nature.* 177:473–475.
43. Oosawa, F., and M. Kasai. 1962. A theory of linear and helical aggregations of macromolecules. *J. Mol. Biol.* 4:10–21.

44. Oosawa, F., and S. Asakura. 1975. Thermodynamics of the Polymerization of Protein. Academic Press, London.
45. Wegner, A. 1976. Head to tail polymerization of actin. *J. Mol. Biol.* 108:139–150.
46. Lee, J. C., and S. N. Timasheff. 1977. In vitro reconstitution of calf brain microtubules: effects of solution variables. *Biochemistry.* 16:1754–1764.
47. Erickson, H. P., and D. Pantaloni. 1981. The role of subunit entropy in cooperative assembly. Nucleation of microtubules and other two-dimensional polymers. *Biophys. J.* 34:293–309.
48. Goldstein, R. F., and L. Stryer. 1986. Cooperative polymerization reactions. Analytical approximations, numerical examples, and experimental strategy. *Biophys. J.* 50:583–599.
49. Weisenberg, R. C. 1986. Kinetic and steady state analysis of microtubule assembly. *Ann. N. Y. Acad. Sci.* 466:543–551.
50. Diaz, J. F., M. Menendez, and J. M. Andreu. 1993. Thermodynamics of ligand-induced assembly of tubulin. *Biochemistry.* 32:10067–10077.
51. Hall, D., and A. P. Minton. 2004. Effects of inert volume-excluding macromolecules on protein fiber formation. II. Kinetic models for nucleated fiber growth. *Biophys. Chem.* 107:299–316.
52. Ferrone, F. A. 2006. Nucleation: the connections between equilibrium and kinetic behavior. *Methods Enzymol.* 412:285–289.
53. Percec, V., G. Ungar, and M. Peterca. 2006. Chemistry. Self-assembly in action. *Science.* 313:55–56.
54. Karsenti, E., and I. Vernos. 2001. The mitotic spindle: a self-made machine. *Science.* 294:543–547.
55. Pollard, T. D., and G. G. Borisy. 2003. Cellular motility driven by assembly and disassembly of actin filaments. *Cell.* 112:453–465.
56. Schmid, M. F., R. Dargahi, and M. W. Tam. 1993. SPECTRA: a system for processing electron images of crystals. *Ultramicroscopy.* 48:251–264.
57. Crowther, R. A., R. Henderson, and J. M. Smith. 1996. MRC image processing programs. *J. Struct. Biol.* 116:9–16.
58. Hardt, S., B. Wang, and M. F. Schmid. 1996. A brief description of I.C.E.: the integrated crystallographic environment. *J. Struct. Biol.* 116:68–70.
59. Valpuesta, J. M., J. L. Carrascosa, and R. Henderson. 1994. Analysis of electron microscope images and electron diffraction patterns of thin crystals of ϕ29 connectors in ice. *J. Mol. Biol.* 240:281–287.
60. Ludtke, S. J., P. R. Baldwin, and W. Chiu. 1999. EMAN: semiautomated software for high-resolution single-particle reconstructions. *J. Struct. Biol.* 128:82–97.
61. Sorzano, C. O., R. Marabini, J. Velazquez-Muriel, J. R. Bilbao-Castro, S. H. Scheres, J. M. Carazo, and A. Pascual-Montano. 2004. XMIPP: a new generation of an open-source image processing package for electron microscopy. *J. Struct. Biol.* 148:194–204.
62. Rivetti, C., M. Guthold, and C. Bustamante. 1996. Scanning force microscopy of DNA deposited onto mica: equilibration versus kinetic trapping studied by statistical polymer chain analysis. *J. Mol. Biol.* 264:919–932.
63. Chiu, W., M. L. Baker, and S. C. Almo. 2006. Structural biology of cellular machines. *Trends Cell Biol.* 16:144–150.
64. Penrose, L. S. 1959. Self-reproducing machines. *Sci. Am.* 200:105–114.
65. Asakura, S. 1968. A kinetic study of in vitro polymerization of flagellin. *J. Mol. Biol.* 35:237–239.
66. Mukherjee, A., and J. Lutkenhaus. 1998. Dynamic assembly of FtsZ regulated by GTP hydrolysis. *EMBO J.* 17:462–469.
67. Howard, J. 2001. Mechanics of Motor Proteins and the Cytoskeleton. Sinauer Associates, Sunderland, MA.
68. Sleytr, U. B., E. M. Egelseer, N. Ilk, D. Pum, and B. Schuster. 2006. S-layers as a basic building block in a molecular construction kit. *FEBS J.* 274:323–334.
69. Gazit, E. 2007. Use of biomolecular templates for the fabrication of metal nanowires. *FEBS J.* 274:317–322.
70. Tadros, M., J. M. Gonzalez, G. Rivas, M. Vicente, and J. Mingorance. 2006. Activation of the *Escherichia coli* cell division protein FtsZ by a low-affinity interaction with monovalent cations. *FEBS Lett.* 580: 4941–4946.
71. Chen, Y., D. E. Anderson, M. Rajagopalan, and H. P. Erickson. 2007. Assembly dynamics of *Mycobacterium tuberculosis* FtsZ. *J. Biol. Chem.* 282:27736–27743.
72. Dajkovic, A., and J. Lutkenhaus. 2006. Z ring as executor of bacterial cell division. *J. Mol. Microbiol. Biotechnol.* 11:140–151.
73. Egelman, E. H. 2003. A tale of two polymers: new insights into helical filaments. *Nat. Rev. Mol. Cell Biol.* 4:621–630.
74. Egelman, E. H. 2006. RecA assembly, one molecule at a time. *Structure.* 14:1600–1602.
75. DiCapua, E., R. W. H. Ruiggrok, and P. A. Timmins. 1990. Activation of recA protein: the salt-induced structural transition. *J. Struct. Biol.* 104:91–96.
76. Mott, M. L., and J. M. Berger. 2007. DNA replication initiation: mechanisms and regulation in bacteria. *Nat. Rev. Microbiol.* 5:343–354.
77. Baxa, U., T. Cassese, A. V. Kajava, and A. C. Steven. 2006. Structure, function, and amyloidogenesis of fungal prions: filament polymorphism and prion variants. *Adv. Protein Chem.* 73:125–180.
78. Diaz-Avalos, R., C. Y. King, J. Wall, M. Simon, and D. L. Caspar. 2005. Strain-specific morphologies of yeast prion amyloid fibrils. *Proc. Natl. Acad. Sci. USA.* 102:10165–10170.
79. Collins, S. R., A. Douglass, R. D. Vale, and J. Weissman. 2004. Mechanism of prion propagation: amyloid growth occurs by monomer addition. *PLoS Biol.* 2:e321.
80. Ban, T., K. Yamaguchi, and Y. Goto. 2006. Direct observation of amyloid fibril growth, propagation, and adaptation. *Acc. Chem. Res.* 39:663–670.
81. Sawaya, M. R., S. Sambashivan, R. Nelson, M. I. Ivanova, S. A. Sievers, M. I. Apostol, M. J. Thompson, M. Balbirnie, J. J. Wiltzius, H. T. McFarlane, A. O. Madsen, C. Riekel, and D. Eisenberg. 2007. Atomic structures of amyloid cross-β spines reveal varied steric zippers. *Nature.* 447:453–457.
82. Ravelli, R. B., B. Gigant, P. A. Curmi, I. Jourdain, S. Lachkar, A. Sobel, and M. Knossow. 2004. Insight into tubulin regulation from a complex with colchicine and a stathmin-like domain. *Nature.* 428: 198–202.
83. Oliva, M. A., D. Trambaiolo, and J. Lowe. 2007. Structural insights into the conformational variability of FtsZ. *J. Mol. Biol.* 373:1229–1242.
84. Ohashi, T., C. A. Hale, P. A. de Boer, and H. P. Erickson. 2002. Structural evidence that the P/Q domain of ZipA is an unstructured, flexible tether between the membrane and the C-terminal FtsZ-binding domain. *J. Bacteriol.* 184:4313–4315.
85. Li, Z., M. J. Trimble, Y. Brun, and G. J. Jensen. 2007. The structure of FtsZ filaments in vivo suggests a force-generating role in cell division. *EMBO J.* 26:4694–4708.